Electronic Supplementary Material (ESI) for Journal of Materials Chemistry A.

Supporting Information:

Insights on the Hydronium-ions Storage of Alloxazine in mild electrolyte

Tianjiang Sun,[a] Chang Liu,[a] XiuFang Xu,[a] Qingshun Nian,[a] Shibing Zheng,[a] Xuesen Hou,[a] Jing Liang,[a] Zhanliang Tao*[a]

[a] Key Laboratory of Advanced Energy Materials Chemistry (Ministry of Education), College of Chemistry, Nankai University, Tianjin 300071, P. R. China.

Corresponding Author

Zhanliang Tao

E-mail: taozhl@nankai.edu.cn

Materials and Equipment

^{1}H NMR and ^{13}C NMR spectra were recorded using AVANCE III 400MHz (Bruker) NMR spectrometers. Chemical shifts were referenced to residual protons or carbons in deuterated solvents. Fourier transform Infrared (FTIR) spectra were recorded for solid samples on a Bruker Tensor II sample compartment RT-DLaTGS spectrometer using attenuated total reflectance (ATR) technique. XPS (Perkin Elmer PHI 1600 ESCA system) was used to characterize the intermediates at various charge/discharge states. Powder X-ray diffraction (XRD) was collected in the wide 2θ range of 10-70° (Rigaku MiniFlex600, Cu Kα radiation). Scanning electron microscopy (SEM) was performed on a SEM, JEOL JSM78500F microscope. Transmission electron microscope (TEM) was performed on a Talos F200X G2, Thermogravimetry (TG) was measured on a thermogravimetric analyzer (NETZSCH, STA 449F3). Cyclic voltammograms were obtained on a Parstat 2263 electrochemical workstation (Princeton Applied Research and AMETEK Company). The discharge/charge tests were conducted on a LAND-CT2001A battery testing instrument.

Electrochemical Measurements

The preparation method of the working electrodes for employing cyclic voltammetry and the galvanostatic discharge/charge tests were described as follows. The cathode electrodes were prepared by mixing 80 wt % MMO with 10 wt % ketjen black (KB) and 10 wt % binder (polytetrafluoroethylene, PTFE) using ethanol as solvent. The ALO anode electrodes were fabricated by mixing 60 wt % ALO with 30 wt % of KB and 10 wt % PTFE. For a typical preparation, ALO and KB were homogeneously blended using agate mortar and pestle. Then PTFE (10% w/w H_2O) and some drops of ethanol were added into the mixture, and the mixture was rolled into small rounds. Using a tablet press, they were rolled into a 1.2 cm diameter circle stainless-steel gauze (Alfa Aesar, 200 mesh woven from 0.05 mm dia wire, Type 304 Wire Cloth). Finally, the as-prepared electrodes were dried at 80 °C in vacuum oven. The mass loading of the active materials in both cathode and anode were 1-2 mg cm^{-2}. The capacity ratio of cathode and anode is about 1.2:1.

The three-electrode system for cyclic voltammetry (CV) consist of MMO or ALO electrodes on stainless steel mesh as working electrode, a large piece of pure platinum as the counter electrode, and silver/silver chloride electrode (Ag/AgCl) as the reference electrode. The electrolyte was 1 M $Mg(NO_3)_2$ aqueous solution. The full batteries with CR2032-type cells were assembled without glovebox using MMO cathode, ALO anode, and 1 M $Mg(NO_3)_2$ as electrolyte. The charge/discharge capacities are based on the mass of the active materials (ALO) in the anode. CV tests were performed using a CHI 660E electro-chemical workstation (ChenHua, Shanghai, China). The first scan of ALO was in a reductive direction and the one of MMO was in an oxidative direction. The discharge/charge tests were conducted on a LAND-CT2001A battery testing instrument. For in situ UV-vis test, we used active carbon (AC) instead of MMO to avoid the influence of the dissolution of manganese ion, the cathode for in situ UV-vis test consisted of 90 wt% AC and 10 wt% PTFE, the anode consisted of 60 wt% ALO, 30 wt% KB and 10 wt% PTFE. For in situ FTIR test, coin-type cell was fabricated with MMO cathode, ALO anode, and 1 M $Mg(NO_3)_2$ electrolyte. The cathode consisted of 80 wt% MMO, 10 wt% KB and 10 wt% PTFE, the anode consisted of 60 wt% ALO, 30 wt% KB and 10 wt% PTFE.

Synthesis of ALO

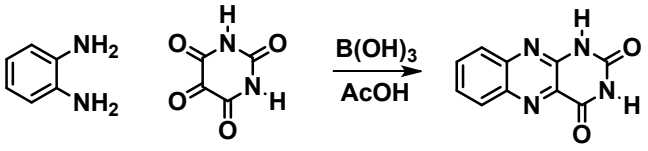

ALO was obtained by one-step reaction at room temperature. In a 50 mL three-necked round bottom flask, *o*-phenylenediamine (3.0 mmol), alloxane monohydrate (3.0 mmol), boric acid (3.0 mmol) and 20 mL acetic acid were added. The mixture was stirred under argon at room temperature for 2 hours. During this time, light yellow solid precipitated out in the solution. The solid was collected by filtrate then washed with 30 mL of acetic acid and 30 mL of diethyl ether. Product was dried further with high vacuum pump. Yield: 87%.

Yield: 87%; Yellow solid, Mp: >400 ºC; ^{1}H NMR (400 MHz, DMSO-d): 7.78 (m, 1H), 7.92 (d, 2H), 8.16 (d, 1H), 11.72 (s, 1H), 11.91 (s, 1H); ^{13}C NMR (75MHz, DMSO-d) δ 161.00, 150.67, 147.40, 143.15,139.71, 133.87, 132.22, 130.66, 128.94, 127.50; FTIR(Neat) 3174, 3105, 3084, 1733, 1688, 1572, 1446, 1272, 1035, 1014, 989, 768, 705, 584, 539, 511, 427, 379 cm^{-1}.

Synthesis of MMO

MMO was prepared by phenol-formalin-assisted sol-gel method. First, magnesium acetate tetrahydrate, manganese acetate tetrahydrate in stoichiometric proportions were completely dissolved in 30 mL of ethanol. 0.5 g phenol and 0.4 mL formalin solution were added into the mixture after being stirred for 30 min at a constant temperature of 60°C. The mixture was stirred for 30 min at 80 °C. After being dried in a vacuum oven at 80 °C for 12 h, the $MgMn_2O_4$ was obtained by calcining for 2 h at 500 °C.

Computational method:

All of the calculations were carried out using the Gaussian 16 program.[1] Geometry optimization and frequency analysis were performed in water solvent with the SMD solvation model using B3LYP functional and 6-311+G(d,p) basis set.[2, 3]

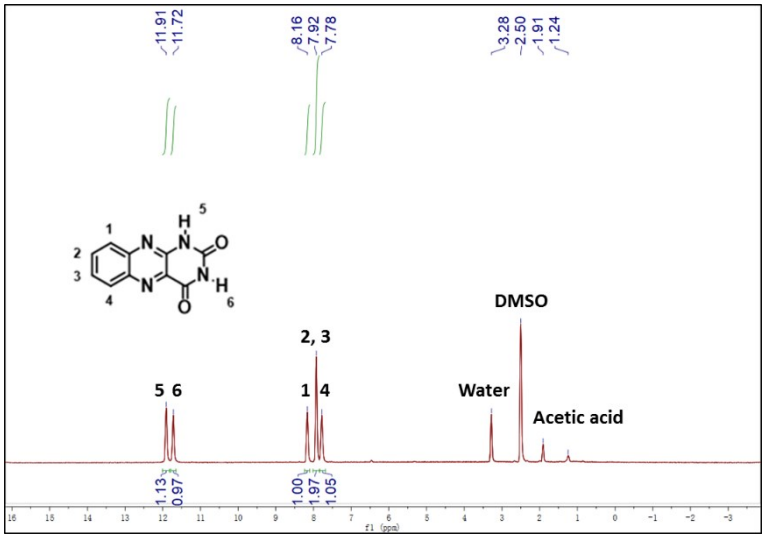

Figure S1 ^{1}H NMR (400 MHz) of ALO in d-DMSO, ^{1}H NMR (400 MHz, DMSO): δ=7.78, 7.92, 8.16, 11.72, 11.91. Total six integrated protons were corresponding to the corresponding hydrogens in ALO. Other peaks should belong to residual solvent: 2.50 ppm (DMSO), 2.95, 1.91 ppm (Acetic acid), 3.28 ppm (water).

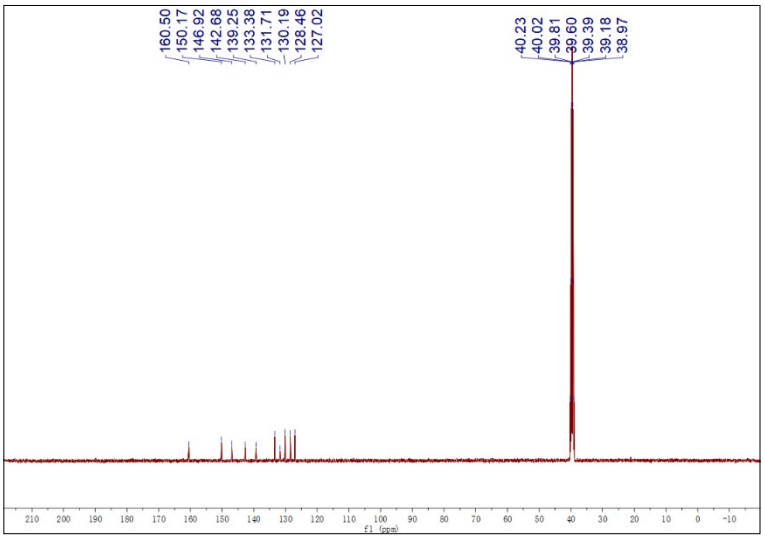

Figure S2 ^{13}C NMR (400 MHz) of ALO in d-DMSO, ^{13}C NMR (400 MHz, DMSO): δ=127.02, 128.46, 130.19, 131.71, 133.38, 139.25, 142.68, 146.92, 150.17, 160.50 ppm. Other peaks should belong to residual solvent: 38.97, 39.18, 39.39, 39.60, 39.81, 40.02, 40.23 ppm (DMSO).

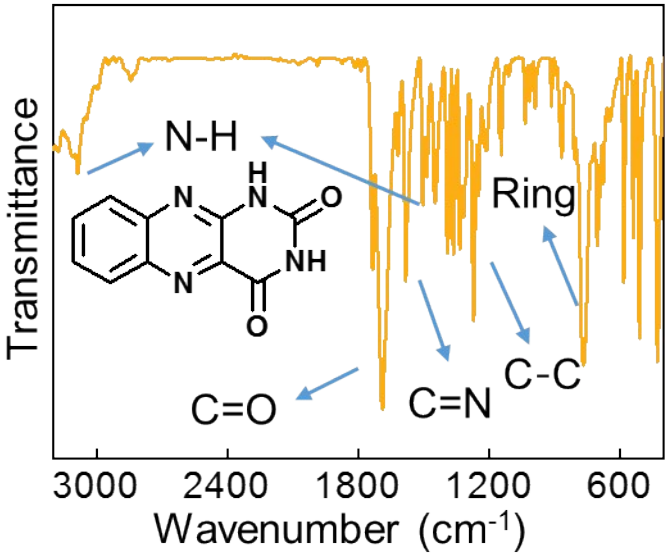

Figure S3 FTIR spectroscopy of as-obtained ALO powder.

From Figure S3, a characteristic signal at 1674 cm^{-1} was observed, corresponding to the typical C=O double bond stretching. Signal at 1581 cm^{-1} belongs to C=N stretching vibration. Signal at 1272 and 760 cm^{-1} belong to C-C stretching vibration in the ring. Signal at 3200 and 1600 cm^{-1} belong to N-H stretching vibration.[4, 5]

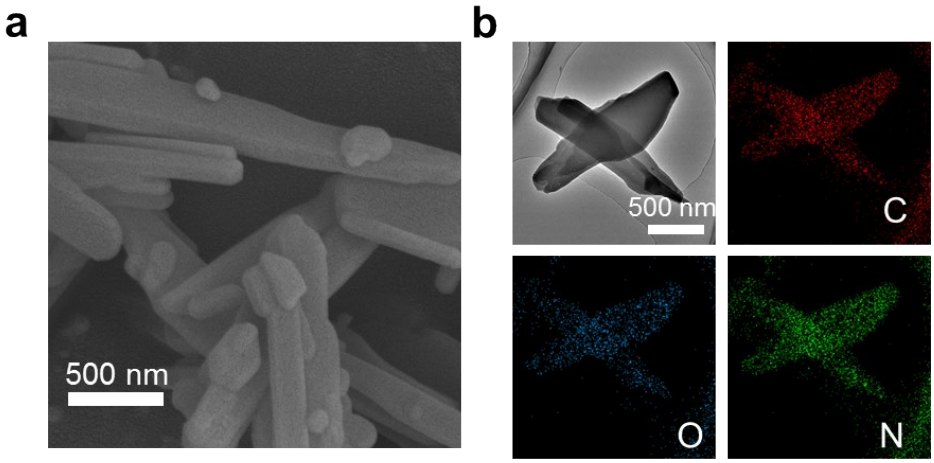

Figure S4 (a) SEM pattern of ALO. (b) TEM-EDS patterns of ALO.

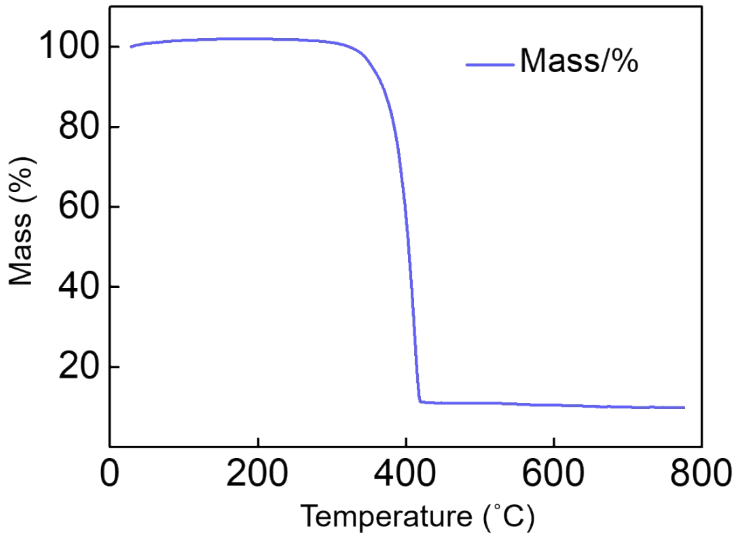

Figure S5 TG curve of ALO in ambient air atmospheres at a heating rate of 5 °C min^{-1}.

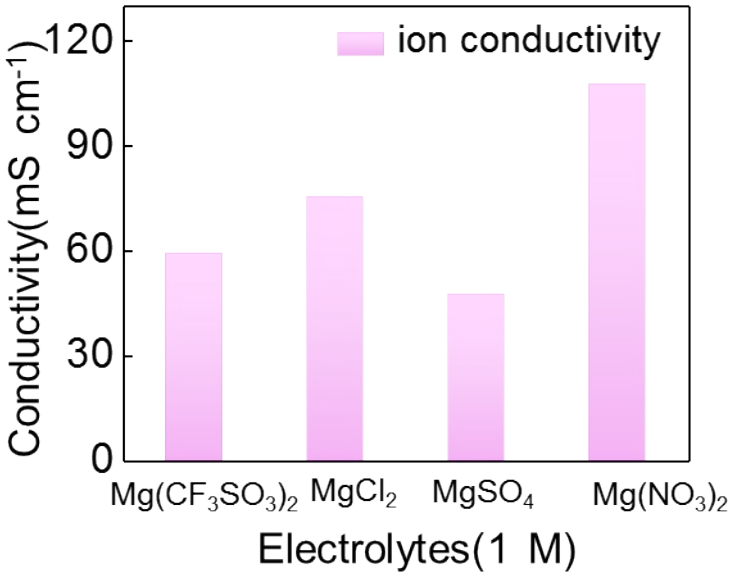

Figure S6 The ion conductivity of different electrolytes.

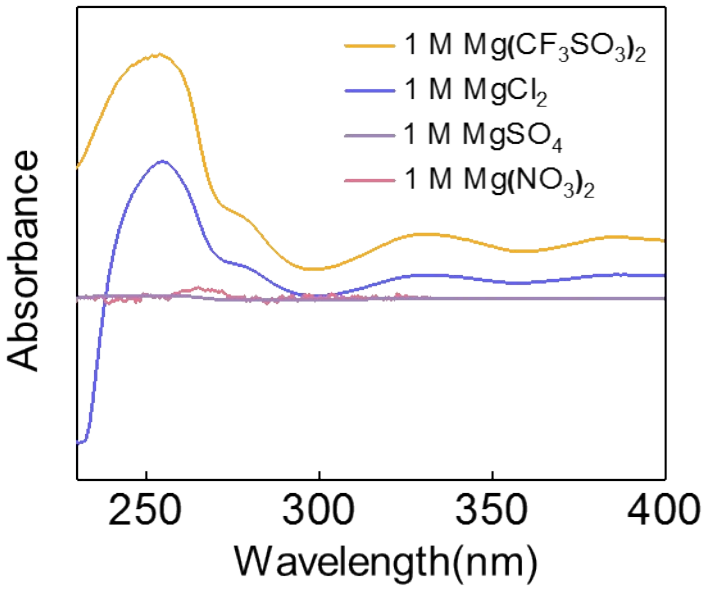

Figure S7 The UV-vis spectroscopy about dissolution of ALO in different electrolytes

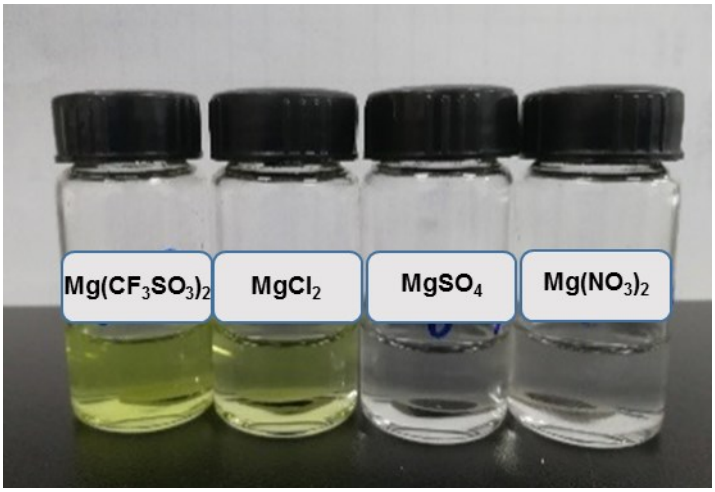

Figure S8 The dissolution of ALO electrode in different electrolytes (standing 24 h).

.

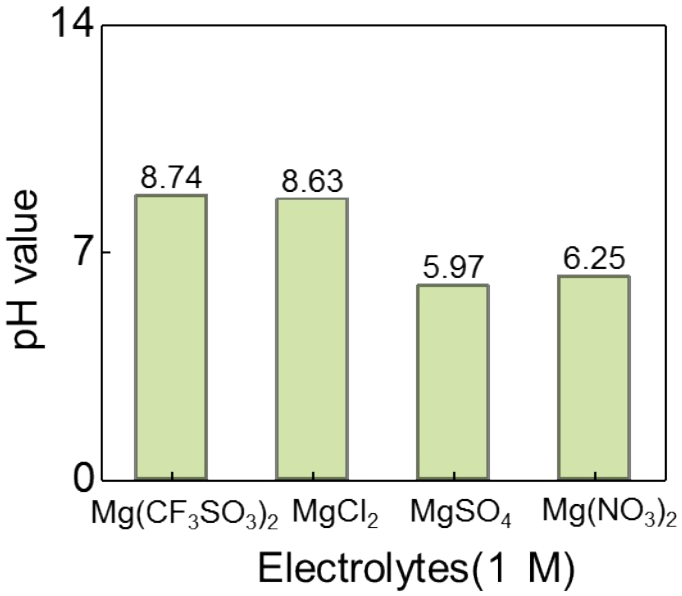

Figure S9 The pH value of different electrolytes.

From Figure S8 and S9, the as-obtained ALO is easily dissolute in alkaline solution.

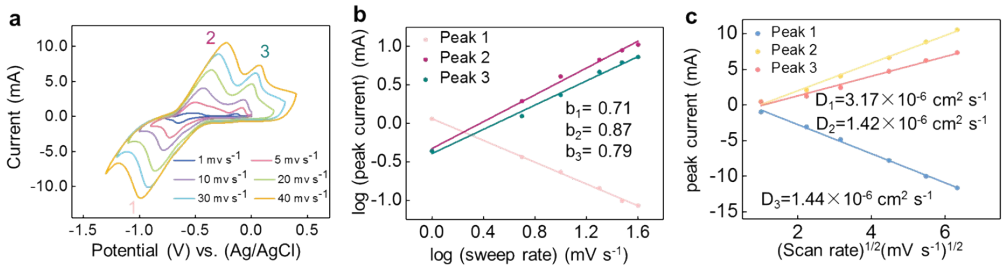

Figure S10 (a) CV curves of ALO electrode in 1 M $Mg(NO_3)_2$ at 1, 5, 10, 20, 30 and 40 mV s^{-1}. (b) Corresponding log peak current vs log sweep rate of ALO electrode. (c) Diffusion coefficients calculated from the CV curves at different scan rates for ALO in 1.0 M $Mg(NO_3)_2$.

From Figure S10, The voltammetry response of ALO at various sweep rates can be summarized according to Eq.1

$$i = av^b \qquad (1)$$

where *a* and *b* are two adjustable parameters, *i* refers to the peak current (mA) and *v* corresponds to sweep rate (mV s^{-1}). The value of *b* shows the mechanism of charge storage. When the value of *b* is 0.5, it suggests the redox reaction is limited by semi-infinite diffusion, which is common in the conventional rechargeable batteries. When the value of $b > 0.5$, is suggests the mechanism is a pseudocapacitor or capacitive behavior, where the rate performance is excellent.

The diffusion coefficient obeys the Equation:

$$i_p = \left(2.69 \times 10^5\right) n^{3/2} A D^{1/2} v^{1/2} C_\circ$$

i_p: Peak current; *n*: Transfer electron number; A: Area of electrode; D: Diffusion coefficients; *v*: scan rates; $C_\circ$: Concentration of ion.

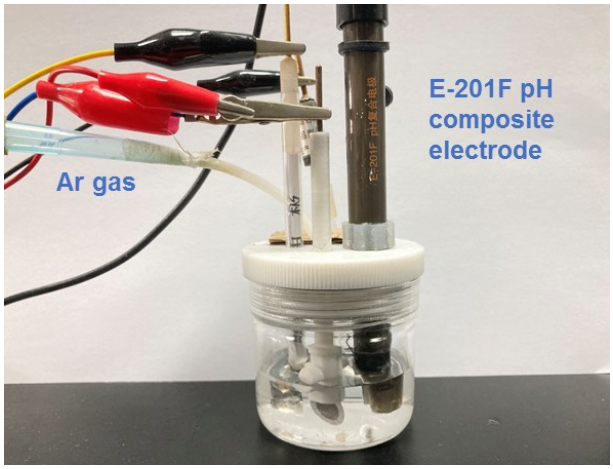

Figure S11 The optical photograph of in-situ pH monitor system.

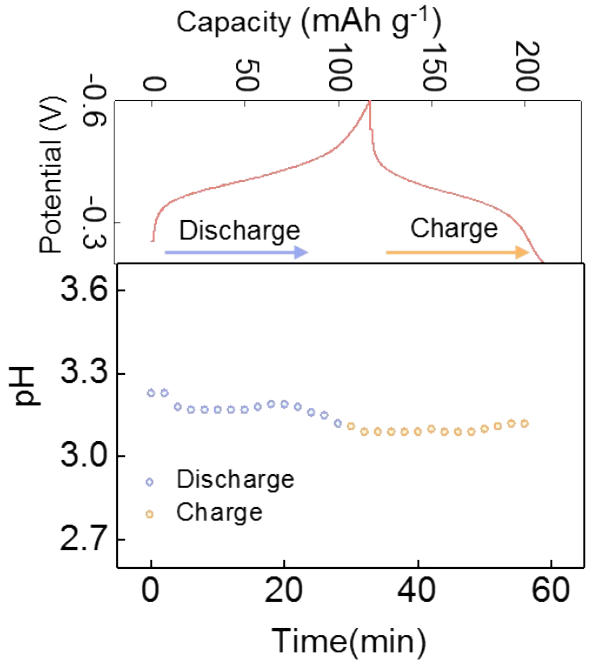

Figure S12 In-situ pH monitor for 1 M $Zn(NO_3)_2$ electrolyte during charging/discharging process (Potential (V vs Ag/AgCl)).

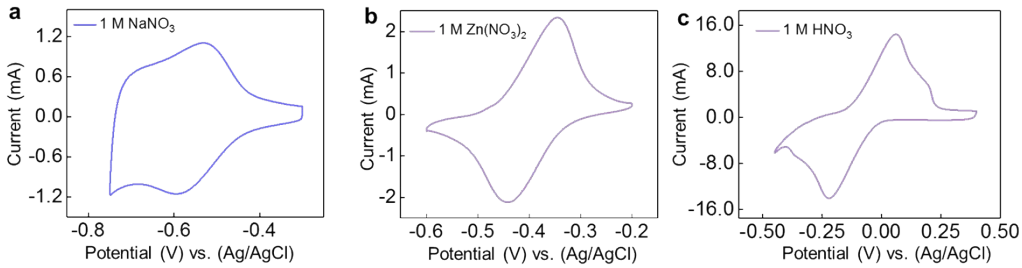

Figure S13 (a) CV curve of ALO electrode in 1 M $NaNO_3$ (1 mV s^{-1}). (b) CV curve of ALO electrode in 1 M $Zn(NO_3)_2$ (1 mV s^{-1}). (c) CV curve of ALO electrode in 1 M HNO_3 (1 mV s^{-1}).

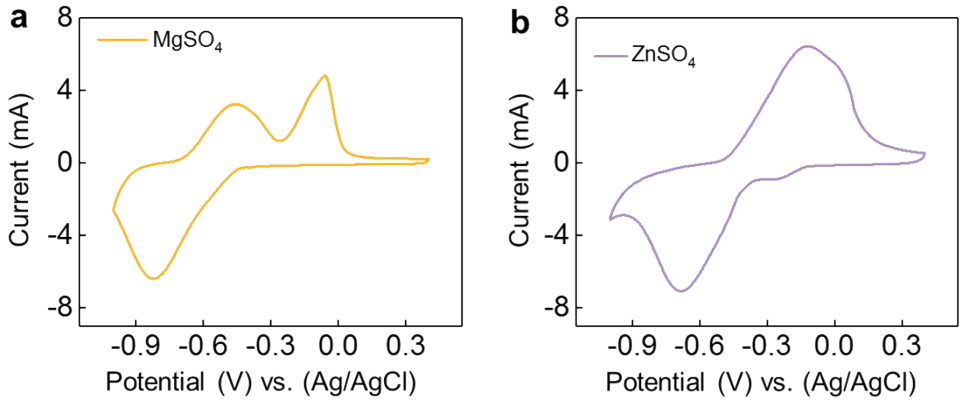

Figure S14 (a) CV curve of ALO electrode in 1 M $MgSO_4$ (1 mV s^{-1}). (b) CV curve of ALO electrode in 1 M $ZnSO_4$ (1 mV s^{-1}).

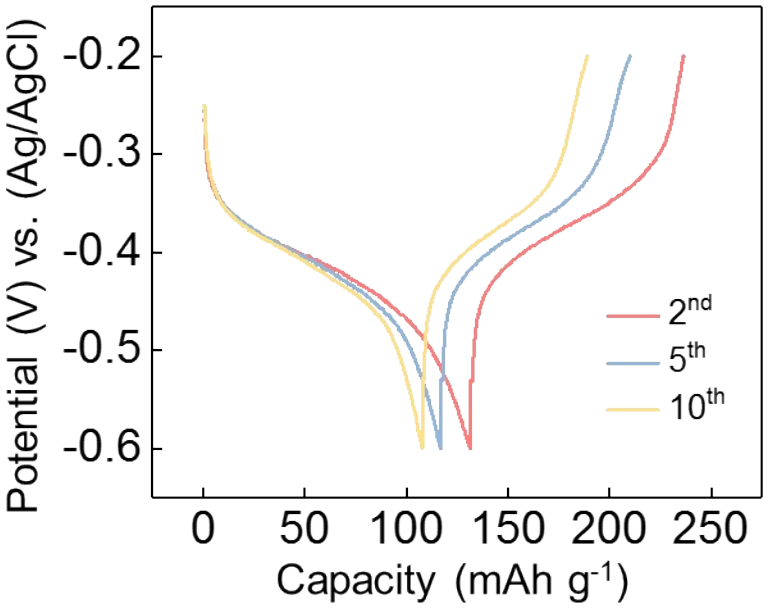

Figure S15 The discharge-charge profile of ALO anode at 1 C (250 mA g^{-1}) in 1 M $Zn(NO_3)_2$ electrolyte.

From Figure S15, the ALO electrode achieves a discharge capacity of 151 mAh g^{-1} at 2nd cycle in 1 M $Zn(NO_3)_2$ electrolyte, and the capacity is rapidly decrease to 107 mAh g^{-1} at 10nd cycle.

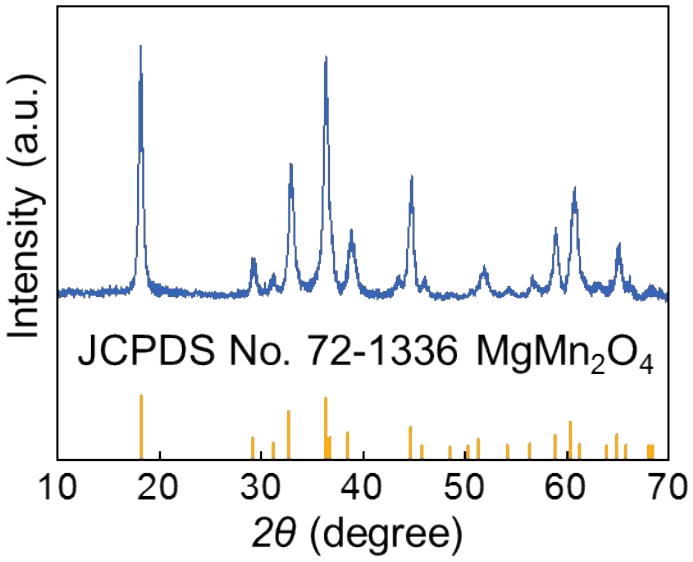

Figure S16 The XRD pattern of MMO.

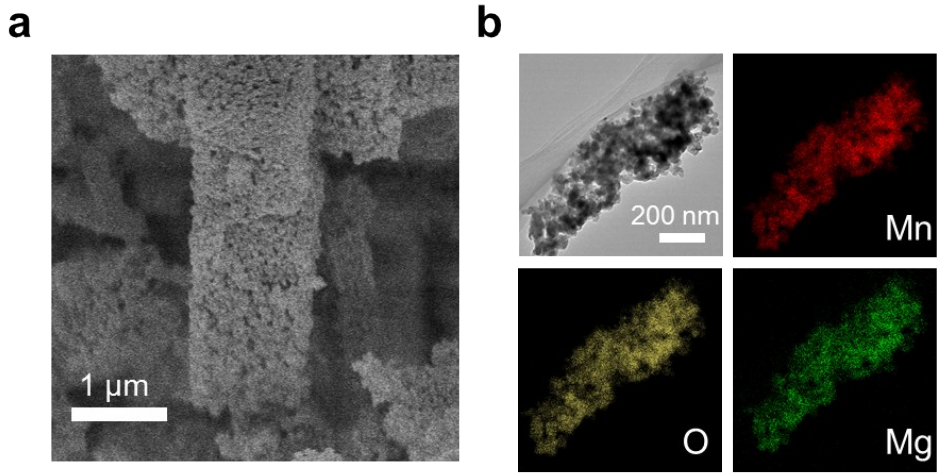

Figure S17 (a) SEM of MMO. (b) TEM and EDS-Mapping of MMO.

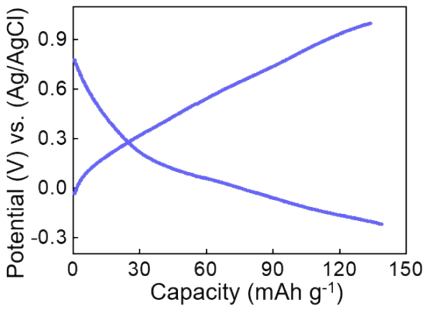

Figure S18 The galvanostatic profile of MMO at current rates of 1 C.

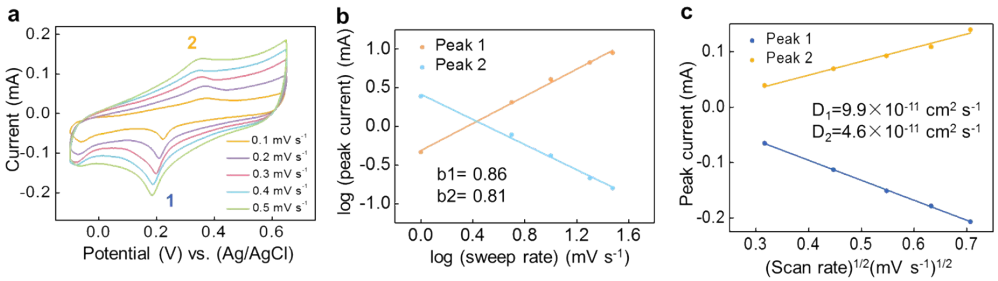

Figure S19 (a) CV curves of MMO electrode in 1 M $Mg(NO_3)_2$ at 0.1, 0.2, 0.3, 0.4, and 0.5 mV s^{-1}. (b) Corresponding log peak current vs log sweep rate of MMO electrode. (c) Diffusion coefficients calculated from the CV curves at different scan rates for MMO in 1.0 M $Mg(NO_3)_2$.

From Figure S19, the calculated b values are 0.86 and 0.81, indicate the electrochemical reaction kinetics is mainly controlled by both diffusion-controlled and surface-controlled capacitive process (Figure S19b). Further, the ion diffusion coefficient was also calculated by CV measurement. As displays in Figure S19c, The Mg^{2+} ion diffusion coefficients of the MMO electrode at Peak 1 and Peak 2 were calculated to be 9.9×10^{-11} cm^2 s^{-1} and 4.6×10^{-11} cm^2 s^{-1}, suggests fast Mg^{2+} ions diffusion on the surface of MMO electrode (Table S3). These results imply good rate performance of MMO cathode.

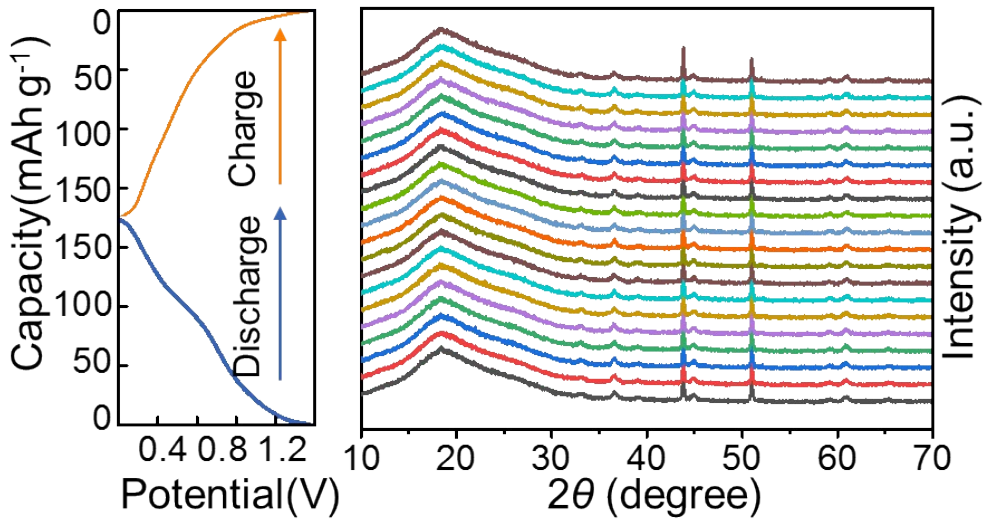

Figure S20 In-situ XRD pattern of MMO electrode during charge and discharge of the full cell.

From Figure S20, the in-situ XRD pattern suggests that MMO has no significant phase transition during charging and discharging processes. The result implies the MMO as a zero-strain cathode material has excellent cycling stability, which is consist with the reported literatures.[7, 8]

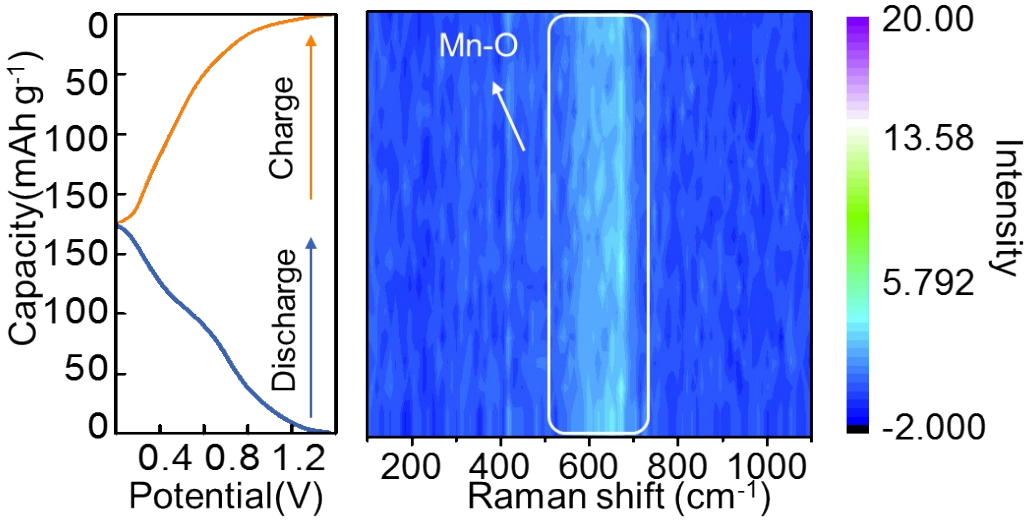

Figure S21 In-situ Raman spectrum of MMO electrode during charge and discharge of the full cell.

From Figure S21, the peak at 667 cm^{-1} corresponds to the signal of Mn-O bond.[9] Obviously, the peak has no change during charging and discharging processes. The in-situ Raman spectrum further confirmed the zero-strain character of MMO during charging and discharging processes.

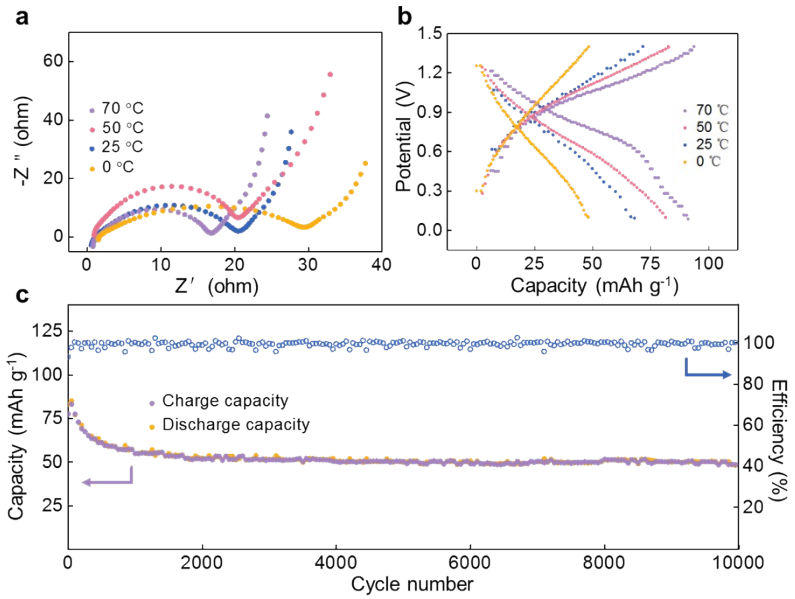

Figure S22. (a) The impedance pattern of ALO//MMO battery at different temperatures. (b) Initial discharge-charge profiles of ALO//MMO battery at different temperatures (at a current density of 20 C). (c) The cycling performance and coulombic efficiency of ALO//MMO battery at 20 C at 70 °C.

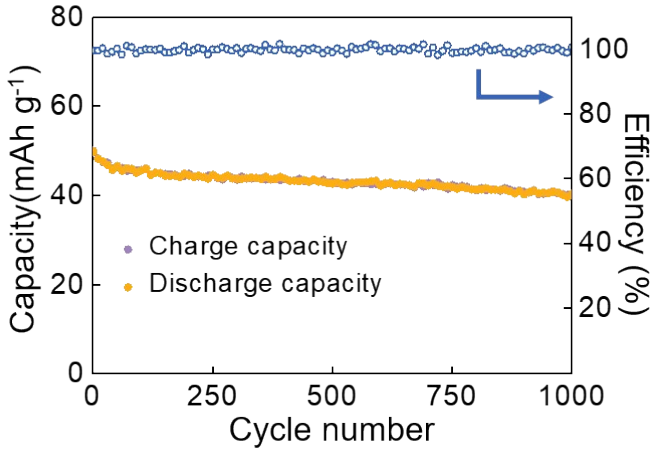

Figure S23 The cycling performance and coulombic efficiencies of ALO//MMO battery at 20 C (5000 mA g^{-1}) at 0 °C.

Table S1 The average potential of materials in different pH-values electrolytes.

Electrode	Electrolyte	Average potential	Corrected potential (V vs Ag/AgCl	Ref
PTO	2.0 M $ZnSO_4$	0.9 V vs Zn^{2+}/Zn	-0.06	[10]
	2.0 M H_2SO_4	0.3 V vs Ag/AgCl	0.3	[11]
PTCDA	1.0 M $LiPF_6$ (EC: DMC= 1: 1Vol %)	2.5 V vs Li^+/Li	-0.7	[12]
	1.0 M H_2SO_4	-0.3 V vs Ag/AgCl	-0.3	[13]
WO_3	1 M $AlCl_3$	-0.4 V vs Ag/AgCl	-0.4	[14]
	0.5 M $Al_2(SO_4)_3$	-0.5 V vs Ag/AgCl	-0.5	
MoO_3	1.0 M H_2SO_4	-0.17 V vs Ag/AgCl	-0.17	[15]
	1.0 M LiOH	-0.9 V vs SCE	-0.85	[16]
	1.0 M H_2SO_4	0 V vs Ag/AgCl	0	[17]
ALO	1.0 M $NaNO_3$	-0.58 V vs Ag/AgCl	-0.58	This work
	1.0 M $Zn(NO_3)_2$	-0.4 V vs Ag/AgCl	-0.4	
	1.0 M $Mg(NO_3)_2$	-0.5 V vs Ag/AgCl	-0.5	
	1.0 M $ZnSO_4$	-0.4 V vs Ag/AgCl	-0.4	
	1.0 M $MgSO_4$	-0.5 V vs Ag/AgCl	-0.5	

Table S2 A comparison of electrochemical performance between this work and reported materials.

Electrode	Electrolyte	Average potential (V vs Ag/AgCl)	Capacity (mAh g^{-1}, A g^{-1})	Cycling stability (capacity retention times)	Ref
PTO	2.0 M H_2SO_4	0.3	151, /	78% after 1000	[11]
PTCDA	1.0 M H_2SO_4	-0.3	70, 1	85% after 150	[13]
MoO_3	1.0 M H_2SO_4	0	257, 100	93% after 200	[18]
MoO_3	1.0 M H_2SO_4	0	146, /	68% after 100	[17]
WO_3	1.0 M H_2SO_4	-0.17	/	87% after 5000	[15]
ALO	1.0 M $Mg(NO_3)_2$	-0.54	159, 5	80% after 2000	This work

Table S3 A comparison of Mg-ions diffusion coefficient between this work and reported aqueous magnesium ion batteries.

Electrode	Electrolyte	D_{Mg2+}/cm^2 s^{-1}	Ref
$MgFe_{1.6}Mn_{0.4}O_4$	0.5 M $MgCl_2$	2.24×10^{-14}	19
$MgFe_{1.33}Mn_{0.67}O_4$		3.26×10^{-13}	
$MgFeMnO_4$		2.89×10^{-13}	
$MgFe_{0.67}Mn_{1.33}O_4$		2.38×10^{-13}	
Mg-OMS-1	0.5 M $MgCl_2$	6.65×10^{-12}	20
	0.5 M $Mg(NO_3)_2$	6.92×10^{-12}	
	0.5 M $MgSO_4$	2.71×10^{-13}	
$MgMn_2O_4$	1 M $Mg(NO_3)_2$	9.90×10^{-11}	This work

Table S4 B3LYP/6-311+G(d,p) calculated energy changes in water solvent.

Reaction	ΔE (eV)
$ALO + H_3O^+ + e^- - H_2O \rightarrow ALO\text{-}H$	-7.145
$ALO\text{-}H + H_3O^+ + e^- - H_2O \rightarrow ALO\text{-}2H$	-7.204
$ALO + 2H_3O^+ + 2e^- - 2H_2O \rightarrow ALO\text{-}2H$	-14.349
$ALO\text{-}2H + Mg^{2+} + H_2O - H_3O^+ - e^- \rightarrow ALO\text{-}Mg^{2+\bullet}$	3.010
$ALO\text{-}Mg^{2+\bullet} - Mg^{2+} + H_2O - H_3O^+ - e^- \rightarrow ALO$	11.339

Reference

1. M. J. Frisch and et.al, Gaussian 09 Revision E.01; Gaussian, Inc.: Wallingford, CT**, 2013.**
2. A. D. Becke, *The J. Chem. Phy.*, 1993, **98**, 5648-5652.
3. C. J. C. Aleksandr V. Marenich, * and Donald G. Truhlar, *J. Phys. Chem. B*, 2009, **113**, 6.
4. L. Zhong, Y. Lu, H. Li, Z. Tao and J. Chen, *ACS Sustainable Chem. Eng.*, 2018, **6**, 7761-7768.
5. B. Tian, Z. Ding, G. H. Ning, W. Tang, C. Peng, B. Liu, J. Su, C. Su and K. P. Loh, *Chem. Commun.*, 2017, **53**, 2914-2917.
6. K. Lin, R. Gómez-Bombarelli, E. S. Beh, L. Tong, Q. Chen, A. Valle, A. Aspuru-Guzik, M. J. Aziz and R. G. Gordon, *Nat. Energy*, 2016, **1**, 16102.
7. J. Yin, A. B. Brady, E. S. Takeuchi, A. C. Marschilok and K. J. Takeuchi, *Chem Commun (Camb)*, 2017, **53**, 3665-3668.
8. Q. D. Truong, M. Kempaiah Devaraju, P. D. Tran, Y. Gambe, K. Nayuki, Y. Sasaki and I. Honma, *Chem. Mater.*, 2017, **29**, 6245-6251.
9. L. Zhao, J. Ni, H. Wang and L. Gao, *RSC Adv.*, 2013, **3**, 6650.
10. Z. Guo, Y. Ma, X. Dong, J. Huang, Y. Wang and Y. Xia, *Angew Chem Int Ed Engl*, 2018, **57**, 11737-11741.
11. Z. Guo, J. Huang, X. Dong, Y. Xia, L. Yan, Z. Wang and Y. Wang, *Nat. Commun.*, 2020, **11**, 959.
12. C. Yuan, Q. Wu, Q. Li, Q. Duan, Y. Li and H.-g. Wang, *ACS Sustainable Chem. Eng.*, 2018, **6**, 8392-8399.
13. X. Wang, C. Bommier, Z. Jian, Z. Li, R. S. Chandrabose, I. A. Rodriguez-Perez, P. A. Greaney and X. Ji, *Angew. Chem. Int. Ed.*, 2017, **56**, 2909-2913.
14. H. Lahan and S. K. Das, *Dalton Trans*, 2019, **48**, 6337-6340.
15. W. Sun, M. T. Yeung, A. T. Lech, C. W. Lin, C. Lee, T. Li, X. Duan, J. Zhou and R. B. Kaner, *Nano Lett*, 2015,

15, 4834-4838.
16. X. Li, J. Shao, J. Li, L. Zhang, Q. Qu and H. Zheng, *J. Power Sources*, 2013, **237**, 80-83.
17. X. Wang, Y. Xie, K. Tang, C. Wang and C. Yan, *Angew. Chem. Int. Ed.*, 2018, **57**, 11569-11573.
18. Y. Deng, Z. Cao, L. Wang, Y. Zhou, S. Fu, Y. Peng, Y. Yin, D. Li, W. Wang, W. Zhou and D. Tang, *Solid State Ionics*, 2020, **353**, 115380.
19. Y. Zhang, G. Liu, C. Zhang, Q. Chi, T. Zhang, Y. Feng, K. Zhu, Y. Zhang, Q. Chen and D. Cao, *Chem. Eng. J.*, 2020, **392**, 123652.
20. H. Zhang, K. Ye, X. Huang, X. Wang, K. Cheng, X. Xiao, G. Wang and D. Cao, *J. Power Sources*, 2017, **338**, 136-144.